ADVANCING EARTH AND SPACE SCIENCE

JGR Atmospheres

RESEARCH ARTICLE

10.1029/2020JD034229

Key Points:

- Co-incident mid- and far-infrared upwelling radiance spectra have been observed from aircraft under clear sky conditions
- Humidity and temperature retrievals show improved information content for the far-infrared over the mid-infrared for these instruments
- This advantage is retained when water vapor only retrievals are performed

Supporting Information:

Supporting Information may be found in the online version of this article.

Correspondence to:

L. Warwick and H. Brindley,
laura.warwick14@imperial.ac.uk;
h.brindley@imperial.ac.uk

Citation:

Warwick, L., Brindley, H., Di Roma, A., Fox, S., Havemann, S., Murray, J., et al. (2022). Retrieval of tropospheric water vapor from Airborne Far-infrared measurements: A case study. *Journal of Geophysical Research: Atmospheres*, *127*, e2020JD034229. https://doi.org/10.1029/2020JD034229

Received 9 NOV 2020
Accepted 23 MAR 2022

Retrieval of Tropospheric Water Vapor From Airborne Far-Infrared Measurements: A Case Study

L. Warwick[1], H. Brindley[1,2], A. Di Roma[3], S. Fox[4], S. Havemann[4], J. Murray[1], H. Oetjen[5], H. C. Price[6], D. Schüttemeyer[5], L. Sgheri[7], and D. A. Tiddeman[4]

[1]Space and Atmospheric Physics, Imperial College London, London, UK, [2]NERC National Centre for Earth Observation, Imperial College London, London, UK, [3]Istituto di Scienze dell'Atmosfera e del Clima, ISAC-CNR, Bologna, Italy, [4]Met Office, Exeter, UK, [5]ESA, ESTEC, Noordwijk, The Netherlands, [6]FAAM Airborne Laboratory, Cranfield, UK, [7]IAC—CNR, Sesto Fiorentino, Italy

Abstract We describe studies undertaken in support of the Far-infrared Outgoing Radiation Understanding and Monitoring mission, European Space Agency's ninth Earth Explorer, designed to investigate whether airborne observations of far-infrared radiances can provide beneficial information on mid and upper tropospheric water vapor concentrations. Initially we perform a joint temperature and water vapor retrieval and show that the water vapor retrieval exploiting far-infrared measurements from the Tropospheric Airborne Fourier Transform Spectrometer (TAFTS) shows improvement over the a-priori Unified Model global forecast when compared to in situ dropsonde measurements. For this case the improvement is particularly noticeable in the mid-upper troposphere. Equivalent retrievals using mid-infrared radiances measured by the Airborne Research Interferometer Evaluation System (ARIES) show much reduced performance, with the degrees of freedom for signal (DFS), reduced by a factor of almost 2. Further sensitivity studies show that this advantage is decreased, but still present when the spectral resolution of the TAFTS measurements is reduced to match that of ARIES. The beneficial role of the far infrared for this case is further confirmed by performing water vapor only retrievals using ARIES and TAFTS individually, and then in combination. We find that the combined retrieval has a DFS value of 6.7 for water vapor, marginally larger than that obtained for the TAFTS retrieval and almost twice as large as that obtained for ARIES. These results provide observational support of theoretical studies highlighting the potential improvement that far-infrared observations could bring for the retrieval of tropospheric water vapor.

Plain Language Summary The Far-infrared Outgoing Radiation Understanding and Monitoring (FORUM) mission has been selected as the European Space Agency's ninth Earth Explorer. Far-infrared Outgoing Radiation Understanding and Monitoring will be the first mission to make high spectral resolution measurements of the Earth's outgoing energy in a region of the spectrum known as the far-infrared. These observations will complement our existing knowledge of the Earth's outgoing spectrum in the mid-infrared, where measurements have been made for many years. This paper describes a study in support of FORUM, using unique aircraft-based observations of far- and mid-infrared spectrally resolved radiation, complemented by measurements of the vertical profile of water vapor and temperature below the aircraft from dropsonde. We infer the humidity and temperature profile from the radiation observations and show that using the far-infrared observations improves our ability to properly capture the observed dropsonde behavior compared to using the mid-infrared measurements alone. This is the first time that far-infrared aircraft observations have been used to demonstrate an improvement in our ability to characterize atmospheric humidity. It suggests that FORUM measurements may be able to enhance our understanding of atmospheric water vapor, with associated benefits for climate prediction.

1. Introduction

Accurately quantifying upper tropospheric (UT) water vapor concentrations is critical for quantifying the Earth's greenhouse effect (Allan et al., 2002; Brindley & Harries, 1998), estimating the strength of water vapor radiative effects and feedback (Dessler et al., 2008; Riese et al., 2012) and characterizing the atmospheric circulation (Pierrehumbert & Roca, 1998), including upper-tropospheric lower-stratospheric exchange mechanisms (Sherwood et al., 2010; Vogel et al., 2014). Measurements of UT water vapor include those performed by radiosonde, aircraft-based sensors and a variety of satellite-based instrumentation operating across the electromagnetic spectrum. However, despite the substantial effort that has been made to assess, improve and homogenize UT water vapor estimates (e.g., McCarthy et al., 2009, 2008; Miloshevich et al., 2006, 2009, 2004; Shi & Bates, 2011) best-case uncertainties from the GCOS Reference Upper Air Network (GRUAN) radiosondes are still of the order 5%, reaching 15% near the tropopause (Dirksen et al., 2014).

Uncertainties are still significant because current measurement techniques have shortcomings over the UT altitude range. Limb sounding instruments, which offer high vertical resolution, are affected by the variable nature of the water vapor horizontal distribution; narrow-band nadir sounding instruments have poor vertical resolution and can suffer from clear sky sampling dry biases (Chung et al., 2014; John et al., 2011); mid-infrared (mid-ir: 667–2000 cm^{-1}) hyperspectral sounders have limited sensitivity to the region and can underestimate humidity extremes (Chou et al., 2009; Fetzer et al., 2008; Trent et al., 2019) and current GPS radio-occultation based approaches have reduced sensitivity in the UT (Kursinski & Gebhardt, 2014). Moreover, while the GRUAN radiosonde measurements are widely recognised as a highly valuable reference data set, providing high vertical resolution, they need corrections to be applied to account for biases induced by daytime solar heating, instrument time-lags and calibration (Dirksen et al., 2014). The sites themselves are also spatially and temporally sparse and are currently not designed to be fully representative of the globe. In situ observations of water vapor concentrations in the UT, derived from instruments on commercial passenger flights under the auspices of the In-service Aircraft for a Global Observing System (IAGOS) project, have been made since 1994 (Petzold et al., 2015). There is no doubt that these data constitute a valuable resource for investigating UT humidity interactions (e.g., Petzold et al., 2017) but they are also restricted in their vertical and latitudinal/longitudinal coverage because of the commercial platforms employed.

Therefore, to better quantify the variability and trends in global UT water vapor and understand their impact on climate, satellite measurements that can provide improved retrieval accuracy with sufficient vertical resolution and global coverage are needed. Theoretical modeling suggests that this may be achievable, at least in part, using spectrally resolved radiance measurements in the far-infrared (far-ir), where clear-sky absorption is dominated by water vapor (Clough et al., 1992; Harries et al., 2008; Merrelli & Turner, 2012; Mertens, 2002; Ridolfi et al., 2020). The far-ir consists of wavenumbers below 667 cm^{-1} (wavelengths >15 μm) and accounts for around 50% of the total outgoing longwave radiation (OLR) globally under all-sky conditions (Harries et al., 2008).

Despite constituting a large percentage of the Earth's OLR, there are currently no space-based instruments capable of measuring spectrally resolved radiances across the far-ir However, two upcoming satellite missions, the European Space Agency (ESA) Far-infrared Outgoing Radiation Understanding and Monitoring (FORUM) mission (Palchetti et al., 2020) and the NASA Polar Radiant Energy in the Far Infrared Experiment (PREFIRE) mission (L'Ecuyer et al., 2021) aim to fill this gap.

The FORUM mission is ESA's 9th Earth Explorer and has a key scientific goal of relating variability in UT water vapor to its radiative signature across the mid- and far-ir. An additional goal is to perform retrievals of the underlying water vapor profile. This paper describes Phase A studies undertaken in support of FORUM designed to investigate whether airborne observations of the far-ir spectrum from aircraft can, in practice, be inverted to provide useful additional information regarding UT water vapor concentrations. The current design goals for the FORUM Sounding Instrument are a spectral coverage of 100–1600 cm^{-1} and a nominal spectral resolution of 0.5 cm^{-1} (full-width half maximum). The goal and threshold noise and absolute radiometric uncertainty are shown in Figure 1 (ESA, 2019). It is worth noting that the characteristics of the airborne instruments used in this study are not the same as those proposed for FORUM, so the results obtained are not directly transferrable to the mission. Nevertheless, the results we present represent, to the best of our knowledge, the first demonstration of mid-upper tropospheric water vapor retrievals from observations of far-infrared spectral radiances. As such, they give a first indication of the likely benefit of the proposed FORUM measurements for water vapor retrievals.

The layout of the paper is as follows: in Section 2 we describe the aircraft campaign, relevant instrumentation and auxiliary data. Section 3 describes the retrieval methodology. Sections 4 and 5 describe water vapor and temperature retrievals performed using far-ir and mid-ir radiance measurements respectively. In Section 6 we consider water vapor retrievals using a fixed temperature profile for a far-ir, mid-ir and combined case with overall conclusions drawn in Section 7.

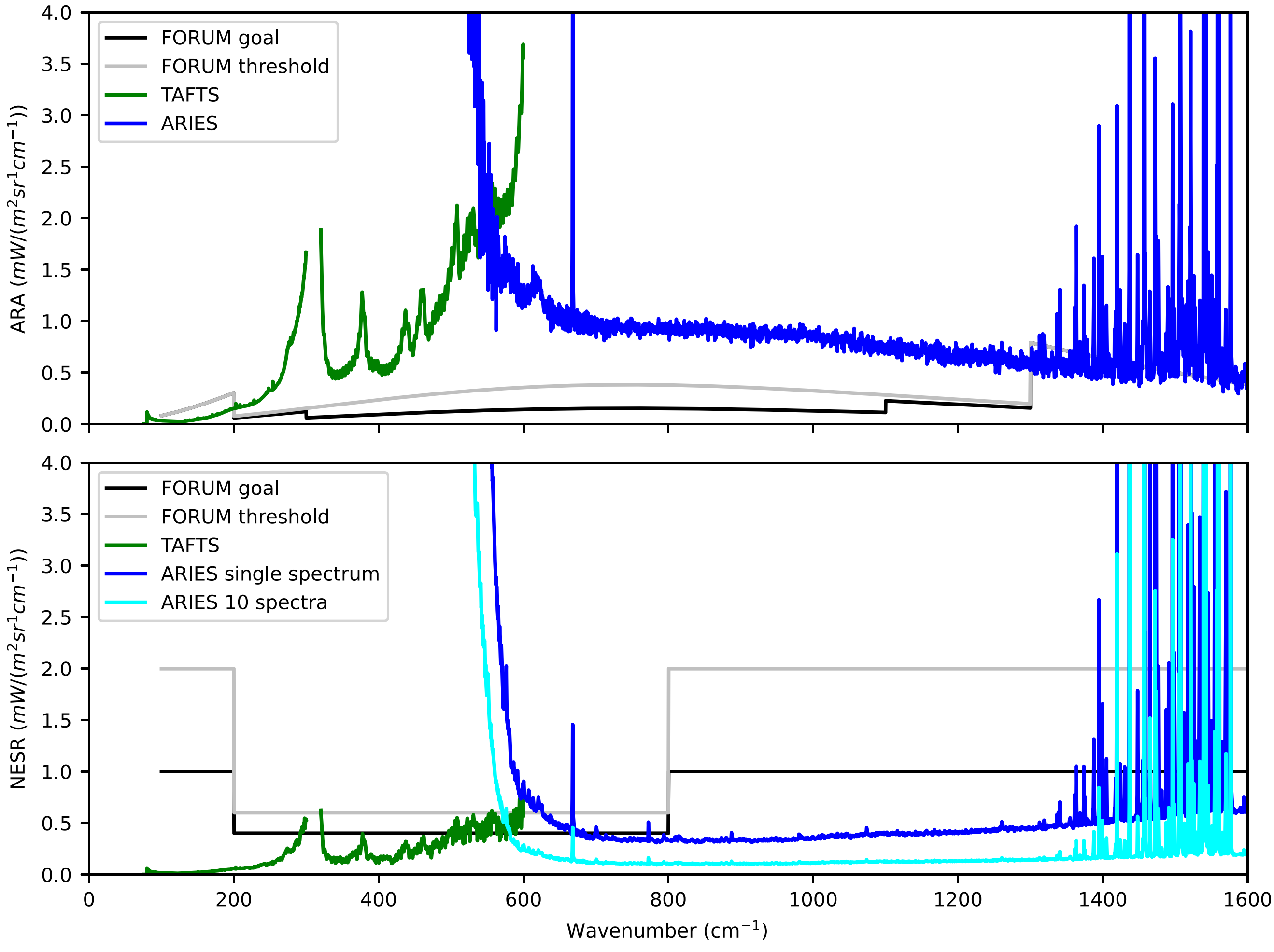

Figure 1. (a) Absolute radiometric accuracy and (b) noise equivalent spectral radiance for Far-infrared Outgoing Radiation Understanding and Monitoring (goal and threshold), Tropospheric Airborne Fourier Transform Spectrometer and Airborne Research Interferometer Evaluation System (ARIES). The random noise for ARIES is shown for both a single spectrum and the 10 average spectra as used in this study.

2. Flight Campaign and Instrumentation

The PIKNMIX-F campaign was a joint endeavor between the UK Met Office and the FAAM Airborne Laboratory, taking place during March 2019 and based out of Stornoway, Scotland. The science goals of the campaign were to obtain data that could be used to improve the representation of specific cloud-microphysical and boundary layer processes within the Met Office suite of models, and to validate radiative transfer modeling of cloudy scenes across the microwave, submillimetre and infrared spectrum. However, additional funding from ESA allowed further dedicated flight hours in support of the FORUM mission.

This paper focuses on flight C153, which took place on 13 March 2019. The goal of flight C153 was to observe co-incident nadir-viewing spectra in the far- and mid-ir from the Tropospheric Airborne Fourier Transform Spectrometer (TAFTS) and the Airborne Research Interferometer Evaluation System (ARIES) at high altitude under clear-sky conditions, coordinated with frequent characterization of the underlying atmospheric state from dropsonde. Following a transit to the operating area over the North Sea (Figure 2), two straight and level runs (SLRs) were carried out between 57 and 55°N from 11:55 UTC to 12:55 UTC. The first SLR was in a southerly direction at around 28,000 ft (8,500 m) and the second returned along nominally the same track in a northerly direction at roughly 30,000 ft (9,100 m). The tracks are shown by the orange line in Figure 2. Dropsonde were periodically released during these two runs from the locations indicated by the stars in the figure. Conditions were generally clear, although there was a small amount of low cloud at the southern end of the run which can be seen in the high-resolution visible channel image from the Spinning Enhanced Visible and InfraRed Imager (SEVIRI)

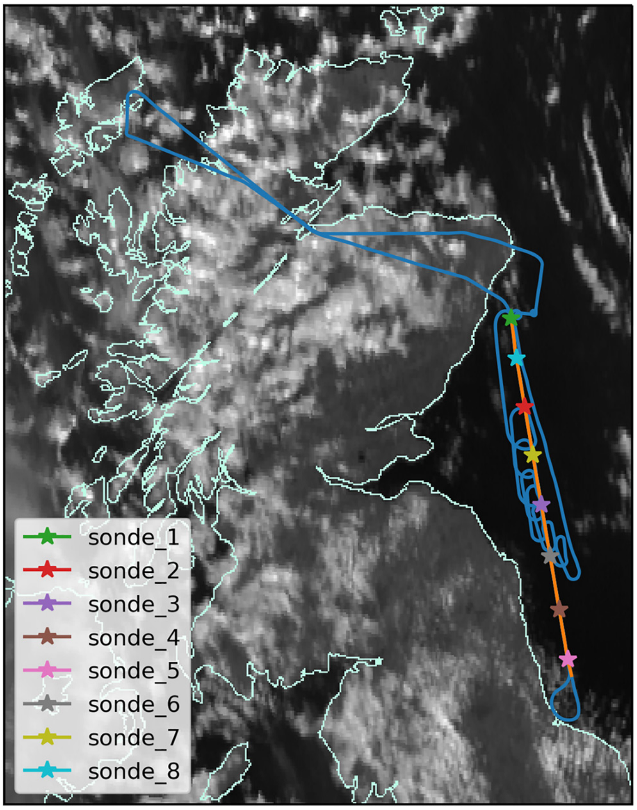

Figure 2. Flight track during C153. The high-altitude legs are shown in orange and the stars mark the dropsonde release locations. The background is the high-resolution visible image from Spinning Enhanced Visible and InfraRed Imager on Meteosat-11 at 12:30UTC.

on Meteosat-11. Following the high-level runs a spiral descent pattern was performed in the vicinity of the central part of the high-level legs, followed by a low-level run at 1000 ft (300 m) prior to the return to Stornoway. During the high-level runs TAFTS and ARIES made coincident measurements of up-welling radiance.

2.1. Radiation Instrumentation

2.1.1. The Tropospheric Airborne Fourier Transform Spectrometer (TAFTS)

TAFTS is a Martin-Puplett polarizing interferometer with a nominal spectral range of 80–550 cm^{-1} (18–125 μm) and a maximum spectral resolution of 0.12 cm^{-1} (Canas et al., 1997). In this study the resolution was reduced to 0.24 cm^{-1} to reduce scan time and make the instrument more robust.

TAFTS is designed in a four-port configuration with two input ports and two output ports. Measurements are made at each output port by pairs of liquid helium cooled photoconductor detectors. Both pairs contain a "longwave" GeGa detector that measures between 80 and 300 cm^{-1} and a "shortwave" SiSb detector that measures from 330 to 550 cm^{-1}. TAFTS also has two pairs of internal blackbody calibration targets. Each pair consists of a cold target held near ambient temperature and a hot target heated to around 323 K. The temperatures of all calibration targets are monitored by platinum resistance thermometers. A single nadir scan by the instrument takes approximately 1.5 s and such scans form part of the overall data acquisition cycle, which consists of internal calibration and external nadir and zenith views.

TAFTS measurement uncertainties contain a systematic and random component related to calibration error and random noise, respectively (Figures 1a and 1b). These random and systematic components are added in quadrature to find the total uncertainty. The measurement uncertainty on a single TAFTS spectrum (80–550 cm^{-1}) increases markedly toward the detector band edges but otherwise is of the order ± 1 mW m^{-2} sr^{-1} $(cm^{-1})^{-1}$ cm^{-1} in the TAFTS shortwave channel and substantially less than this in the TAFTS longwave channel.

2.1.2. The Airborne Research Interferometer Evaluation System (ARIES)

ARIES is a Michelson-type interferometer with a spectral range of 550–3,000 cm^{-1} (3–18 μm) and a spectral resolution of 1 cm^{-1} (Wilson et al., 1999). To cover this spectral range, ARIES makes use of two photodetectors, the first is a HgCdTe photodetector covering 550–1800 cm^{-1}, the second is InSb with a range from 1700 to 3000 cm^{-1}. ARIES also contains two temperature-controlled blackbody targets, which are monitored by platinum resistance thermometers. ARIES uses these targets to perform regular calibration views during measurements. A single scan of the ARIES instrument takes 0.25 s.

The ARIES measurement errors also consist of a systematic (Figure 1a) and random component (Figure 1b). In this study, we use an average of 10 consecutive ARIES spectra to make the TAFS and ARIES spectra more comparable in both acquisition time and total uncertainty. This reduces the random component of the ARIES uncertainty (Figure 1b) but has little impact on the total uncertainty at wavenumbers between 600 and 1600 cm^{-1} because of the dominance of calibration uncertainties. To make the TAFTS/ARIES instrument combination more comparable to a FORUM-type measurement we only use ARIES data at wavenumbers up to 1600 cm^{-1}.

2.2. Auxiliary Data

Additional data to characterize the atmospheric state were taken from the core instruments on board the FAAM aircraft (FAAM Instrument Team, 2019). Positional information was measured by the POS AV 410 GPS-aided

Table 1
L2M_I Settings for the Retrievals in This Paper

L2M_I general settings for this paper	
Max. number of Levenberg-Marquardt iterations	10
Max. number of Gauss-Newton iterations	5
Initial value for λ parameter	0.1
λ reduction factor if LM iteration successful	5
λ multiplicative factor if LM iteration failed	5
Maximal relative variation of the chi-square to achieve convergence	0.01
Maximal relative variation of the parameters to achieve convergence	0.01

Inertial Navigation unit. Static air temperature was derived from measurements made using a Rosemount Aerospace Inc. Type 102 De-iced Total Temperature Housing fitted with an IST MiniSens PRT sensor, and the Air Data Computer on G-LUXE (BAE Systems., 2000). The water vapor volume mixing ratio was derived from dewpoint measurements made using a Buck Research Instruments CR2 Chilled Mirror Hygrometer with heated inlet and information from the Air Data Computer. Flight level ozone concentrations were recorded by a Core Thermo Fisher Scientific Inc. Model 49i UV absorption ozone photometer (hereafter TECO 49) and static pressure was recorded by the Air Data Computer.

During the high-level part of the flight described here the Advanced Vertical Atmospheric Profiling System on the aircraft periodically released Vaisala RD94 dropsonde, providing measurements of the atmospheric profile below the aircraft. Miloshevich et al. (2009) assessed the uncertainty in humidity measurements from the Vaisala RS92 radiosonde which uses the same humidity sensor as the Vaisala RD94. This uncertainty was assumed to have two components arising from sensor calibration and production variability. The former was estimated as ±5% of the measured relative humidity value plus an absolute offset of ±0.5%, the latter as ±1.5% of relative humidity values above 10% or ±3% for values below 10%. As there is no similar information available for the temperature measurement, the manufacturer quoted repeatability of 0.2 K is used to represent the uncertainty, though it should be noted that this may not capture any bias present in the measurement (Vaisala, 2017).

We also make use of the global forecast from the operational Met Office Unified Model (UM; Walters et al., 2017). This model configuration has 70 levels and a grid length of 10 km in the midlatitudes. The background error covariance matrix (B-matrix) for the UM is symmetric, positive definite and has 144 elements (rows/columns) in total. These correspond to the correlated errors in temperature and specific humidity on each of the vertical levels. The remaining four elements of the B-matrix are the errors in the near surface air temperature, near surface humidity, surface pressure and the surface skin temperature, however of these elements only the skin surface temperature is used in this study.

3. Retrieval Methodology and Evaluation Metrics

The retrievals were performed using the L2M_I (Level 2 Module – Inversion) code, which was written for the FORUM End-to-End simulator ESA project (Sgheri et al., 2021). This is a standalone software for the solution of the inverse radiative transfer problem in clear or cloudy sky conditions and can perform estimates of selected geophysical parameters including surface temperature and emissivity, and vertical profiles of atmospheric temperature and volume mixing ratios of several gaseous species. The code can also perform joint retrievals from co-located observations from up to 5 different sensors. The retrieval algorithm is based on the Optimal Estimation method (Rodgers, 2000), exploiting the Gauss-Newton (GN) iterative procedure with the Levenberg optimization introduced to prevent occasional convergence failure of the GN scheme in non-linear problems. Thus, the single iterative step of the retrieval algorithm updates the retrieval state vector with the following formula:

$$\mathbf{x}_{k+1} = \mathbf{x}_k + \left(\mathbf{K}_k^t \mathbf{S}_y^{-1} \mathbf{K}_k + \mathbf{S}_a^{-1} + \lambda_k \mathrm{diag}\left(\mathbf{K}_k^t \mathbf{S}_y^{-1} \mathbf{K}_k\right)\right)^{-1} \left[\mathbf{K}_k^t \mathbf{S}_y^{-1} (\mathbf{y} - \mathbf{F}(\mathbf{x}_k)) + \mathbf{S}_a^{-1} (\mathbf{x}_a - \mathbf{x}_k)\right]$$

where k is the iteration index, $\mathbf{x}_k$ is the retrieval state vector, λ_k is the Levenberg-Marquardt parameter, $\mathbf{K}_k$ is the Jacobian matrix, $\mathbf{S}_y$ is the Variance-Covariance Matrix of the measurements and $\mathbf{x}_a$ is the a-priori with Variance-Covariance Matrix $\mathbf{S}_a$. The inversion starts from an initial guess $\mathbf{x}_0$, which in the case of this paper is equivalent to $\mathbf{x}_a$, and the sequence is iterated until the achievement of one or more convergence criteria, or when a maximum user defined number of iterations is reached. Then, the IVS (Iterative Variable Strength) regularization technique (Ridolfi & Sgheri, 2011) is applied to smooth out the retrieved profiles. The specific settings for these retrieval tests are listed in Table 1.

The simulated spectrum and Jacobians at each step are calculated by the Forward Model of the L2M_I package, consisting of version 12.8 of the Line-By-Line Radiative Transfer Code (LBLRTM, Clough et al., 2005). These

10.1029/2020JD034229

are computed at high spectral resolution (0.001 cm^{-1}), then convolved with an externally provided instrumental spectral response function to obtain the simulated spectra and Jacobians at the instrumental spectral resolution.

At the time of running these tests the input structure of the L2M_I code did not allow the specification of the variance-covariance matrix of the a-priori state from an external file; thus the Met Office B-Matrix could not be inserted directly into the retrieval code. Therefore, the Met Office B-Matrix was analyzed to define the a-priori error of each retrieved parameter and a correlation length for temperature and water vapor that would reproduce the B-matrix as accurately as possible. This correlation length was found to be 0.8 km for both variables. The cross-correlation between temperature and water vapor could not be included and so was assumed to be zero given that it was many orders of magnitude smaller than the correlation within the temperature and water vapor profiles. Plots showing the constructed a-priori variance-covariance matrices for temperature and water vapor can be found Figure S1 in Supporting Information S1.

We use several parameters to assess the performance of the retrievals. The first is the degrees of freedom of signal (degrees of freedom for signal [DFS]). This is defined as the trace of the averaging kernel matrix ($\boldsymbol{A}$) and represents the number of independent pieces of information in a set of measurements. The averaging kernel represents the sensitivity of the retrieval to different atmospheric layers and is calculated by:

$$\boldsymbol{A} = \left(\boldsymbol{K}^t \mathbf{S}_y^{-1} \mathbf{K} + \mathbf{S}_a^{-1}\right)^{-1} \boldsymbol{K}^t \mathbf{S}_y^{-1} \boldsymbol{K}$$

The second parameter we use is the root mean squared error (RMSE) which is calculated using the difference between the a-priori or retrieved profile and the nearest dropsonde profile, which for this analysis we assume represents the true atmospheric profile. As the water vapor concentration varies by several orders of magnitude over the height of the profile, we calculate the RMSE values for water vapor using the units of the logarithm of specific humidity, which also has the benefit of being a more appropriate measure of water vapor radiative impact (Soden & Bretherton, 1993). The RMSE is also split into different height regions to assess the vertically resolved performance of the retrieval. It should be noted that conclusions about the performance of the retrieval inferred from the RMSE values may be specific to the atmospheric conditions sampled in this study, however the DFS values should be more generally applicable for instruments with similar uncertainty characteristics.

4. Water Vapor and Temperature Retrievals From TAFTS

4.1. Initial Retrieval

Retrievals of atmospheric temperature, water vapor and skin surface temperature were performed using the TAFTS spectrum recorded closest to the release of dropsonde 8 at 12:51 UTC. The a-priori humidity and temperature profiles and skin surface temperature were taken from the T+1 hr global forecast from the operational Met Office UM at an initialization time of 12UTC (Walters et al., 2017), with values extracted for the closest grid-point to the aircraft observations without spatial or temporal interpolation. In this case the aircraft was 3 km from the center of the grid box when the dropsonde was released.

The surface emissivity in all retrievals was fixed having been derived using an iterative method based on one of the Radiative Transfer for TOVS (RTTOV) ocean emissivity models: IREMIS (Saunders et al., 2017). In IREMIS the spectral emissivity (spanning 100–3,300 cm^{-1}) is parameterized as a function of surface skin temperature, surface wind speed and sensor viewing zenith. For this study, an emissivity spectrum was first generated using an initial guess of skin surface temperature, a sensor zenith angle of 0° and zonal and meridional wind speeds of 10 m s^{-1} and 3 m s^{-1}, respectively. Below 100 cm^{-1} an emissivity of one was assumed. This initial surface emissivity spectrum, together with the temperature and water vapor profiles measured by dropsonde 7, was used as input to the line-by-line version of the Havemann-Taylor Fast Radiative Transfer Code (HT-FRTC; Havemann et al., 2018) to simulate ARIES radiances. The simulated radiances were compared with ARIES observations in the window region between 880 and 920 cm^{-1} and the surface skin temperature (and hence emissivity spectrum) iteratively adjusted until the RMS difference between the observations and simulation was minimized. The best fit was seen with a surface skin temperature of 280.25 K. A further match-up between simulations and observations at the time of the nearest low-level aircraft run yielded the same estimate for the surface skin temperature, giving confidence in the derived emissivity spectrum.

10.1029/2020JD034229

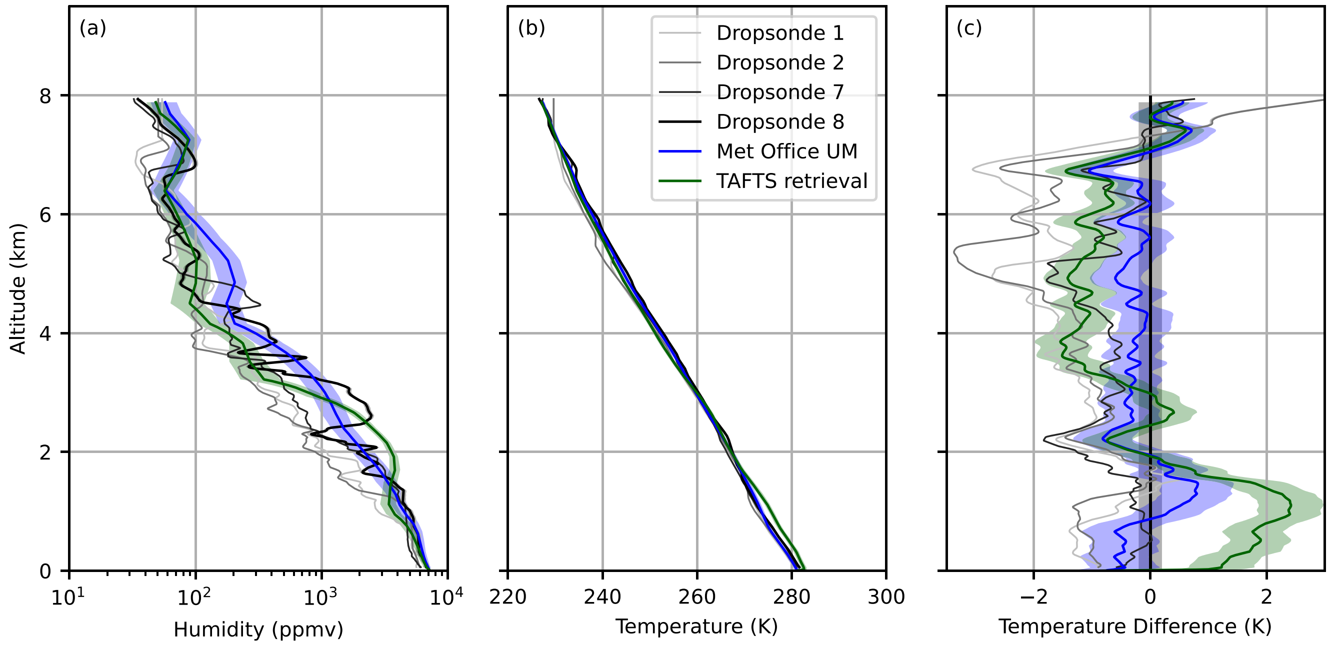

Figure 3. (a) Water vapor and (b) temperature retrievals performed using Tropospheric Airborne Fourier Transform Spectrometer radiances. The shading around the line represents the uncertainty in the retrieval taken from the diagonal elements of the a-posteriori error covariance matrix. The blue line is the a-priori profile taken from the Met Office UM and the blue shading the uncertainty in the a-priori profile taken from the diagonal elements of the a-priori error covariance matrix. The gray lines are profiles recorded by dropsonde 1, 2, and 7. The black line is the profile measured by dropsonde 8 with the gray shading representing the limits of the measurement uncertainty, which is significantly smaller than the a-priori or retrieval uncertainty. Panel (c) shows the differences of the a-priori, retrieved temperature and dropsonde profiles from dropsonde 8.

Figure 3 shows the water vapor and temperature retrievals, the initial a-priori profiles and four dropsonde profiles. Dropsonde 8 was released closest both spatially and temporally to the radiance measurements. We therefore use this as our estimate for the true atmospheric state. However, dropsonde 8 drifted a total of 17 km south-east over approximately 10 min after it was released from the aircraft. The aircraft also traveled 250 m while the spectra were taken. Therefore, to assess the variability of the atmosphere we also examined the water vapor and temperature profiles for dropsonde 1, 2 and 7. Dropsonde 1 and 2 were released closest to dropsonde 8 spatially, at around 30 km away but around an hour prior. Dropsonde 7 was released 9 min before dropsonde 8 but over 60 km away (see Figure 2).

The profiles from dropsonde 1 and 2 are cooler than profiles 7 and 8 above 3 km, suggesting that the atmosphere in this region warmed slightly over the course of an hour. The a-priori temperature profile from the UM forecast and that measured by dropsonde 8 generally agree within their respective uncertainties, with the UM typically colder than the dropsonde. The water vapor measurements for all four dropsonde have more vertical structure than the UM profile however in the mid-upper troposphere (specifically 5–6 km) all 4 dropsonde measure a drier atmosphere than is predicted by the UM. Dropsonde eight includes a notable moist layer at around 3 km which is not present in the UM or the other dropsonde. There is thus the possibility that this wet layer is very localized.

The TAFTS humidity retrieval captures the drier layer in the mid-upper troposphere well, with the retrieved profile moving away from the a-priori UM profile toward the profile of dropsonde 8. However, below 3 km the humidity retrieval is not an improvement over the a-priori and the retrieval does not capture the moist layer at 3 km, instead producing a moist layer lower in the atmosphere which is not present in any of the dropsonde measurements. A positive bias reaching over 2 K is also apparent in the temperature retrieval across the 0–2 km height range. Conversely the retrieved temperature profile is colder than both the a-priori and dropsonde 8 between 3 and 7 km. The 2 K difference between the retrieval and dropsonde below 2 km is larger than the maximum difference seen between the temperature profiles of dropsonde 7 and 8 suggesting that this difference cannot be explained by atmospheric variability.

Table 2
Root Mean Squared Error Values for the Retrievals in Section 4.1

	Water vapor (log (kg/kg))		Temperature (K)	
RMSE	Met office UM	Retrieval	Met office UM	Retrieval
Overall	0.42	0.40	0.44	1.23
0–2 km	0.11	0.28	0.50	1.72
2–4 km	0.50	0.61	0.42	0.84
4–6 km	0.63	0.34	0.33	1.15
6–8 km	0.31	0.24	0.46	0.70

Note. Root mean squared error (RMSE) values are shown for the retrieval of water vapor and temperature with respect to the dropsonde values. The RMSE values for the a-priori are also shown (Met Office UM).

This visual impression of retrieval performance is confirmed by examining the RMSE values for the water vapor and temperature retrievals and a-priori profiles (Table 2) compared to dropsonde 8. Overall, the water vapor retrieval is closer to the dropsonde profile than the a-priori UM profile, with the improvement mainly occurring between 4 and 8 km. Below 4 km the retrieval is further from the dropsonde than the a-priori. The temperature retrieval is not an improvement over the a-priori with the 0–2 km section having a particularly large RMSE.

4.2. Forward Modeling

To investigate the behavior of the retrieval, forward modeling of the observed radiances was performed. These simulations were also carried out using LBLRTM v12.8. One simulation, denoted "UM", used the profiles and surface temperature from the UM forecast as per the a-priori in Section 4.1. The same fixed surface emissivity spectrum was also used. A second simulation combined the temperature and humidity profiles observed by dropsonde 8 and the in situ temperature, humidity and pressure measurements made at the aircraft level to construct inputs for a "dropsonde" simulation. In this case a gap of around 800 m between the altitude of the aircraft and start of the dropsonde measurements was filled using the corresponding UM profile, which did not require scaling to be consistent. The final profile had 128 levels with a vertical resolution of 80 m, chosen to capture the structure of the dropsonde measurements. The surface temperature used for this case was 280.25 K as obtained from IREMIS when calculating the surface emissivity. In both cases an ozone profile was constructed using the in situ data recorded by the aircraft's TECO 49 instrument during the spiral descent later in the flight. CO_2 concentrations were assumed to follow a standard mid-latitude winter profile (Anderson et al., 1986), scaled by the atmospheric concentration of CO_2 on the day of the flight as reported by NOAA/ESRL which in this case was 410.6 ppm (Dlugokencky et al., 2019).

To estimate the effect of uncertainty in the temperature and humidity profiles on the simulated radiances, two additional simulations were performed for each case. These simulations were designed to give an upper and lower bound on the simulated spectra. For the UM case the simulations were constructed by applying a height dependent offset to the temperature and humidity profiles. This offset was determined from the diagonal elements of the UM B-matrix. For the dropsonde model, offsets to the humidity and temperature profiles were applied in line with the estimated dropsonde measurement uncertainties (see Section 2.2).

Using LBLRTM, nadir radiances were generated at high resolution from 50 to 1600 cm^{-1}. These radiances were then Fourier-transformed and apodised with the TAFTS instrument response function before being re-transformed and sampled at the TAFTS wavenumber scale. The resulting simulated spectra for the UM and dropsonde cases are shown in Figure 4 along with the measured radiance.

Figure 5 shows the difference between the simulated radiances and the TAFTS measurements for each case. The shading around each line captures the impact of the temperature and humidity perturbations described above, combined with the TAFTS total measurement uncertainty as illustrated in Figure 2.

In the TAFTS longwave channel the UM and dropsonde simulations are visually similar (Figure 5a). Differences in this region, and within the shortwave channel, are most marked within micro-windows, between 220 and 550 cm^{-1} (e.g., 230, 325, 390, and 420 cm^{-1}). In most micro-windows the dropsonde simulation is a better match to the measured radiances. Moreover, between 320 and 400 cm^{-1} the UM simulation tends to show a negative bias that is less marked in the dropsonde case. This improved agreement is consistent with the retrieved water vapor profile moving toward the dropsonde profile from the UM a-priori in the retrieval. However, in both models there is a negative bias of 3–5 mW m^{-2} sr^{-1} $(cm^{-1})^{-1}$ cm^{-1} between 440 and 520 cm^{-1}. The shape of this bias is similar in both cases suggesting either a systematic effect across both simulations or a bias in the measurements. Additional sensitivity analyses (see Supporting Information Text S2 and Figures S4–S7) indicate that realistic perturbations to surface temperature and emissivity cannot be entirely responsible. Water vapor spectroscopic uncertainty is another possible cause, however realistic perturbations to the strength of the foreign-broadened water vapor continuum in line with the estimated uncertainties in Mlawer et al. (2019) and to the water vapor line widths as specified in the HITRAN 2012 spectroscopic line database (Rothman et al., 2013) are unable

10.1029/2020JD034229

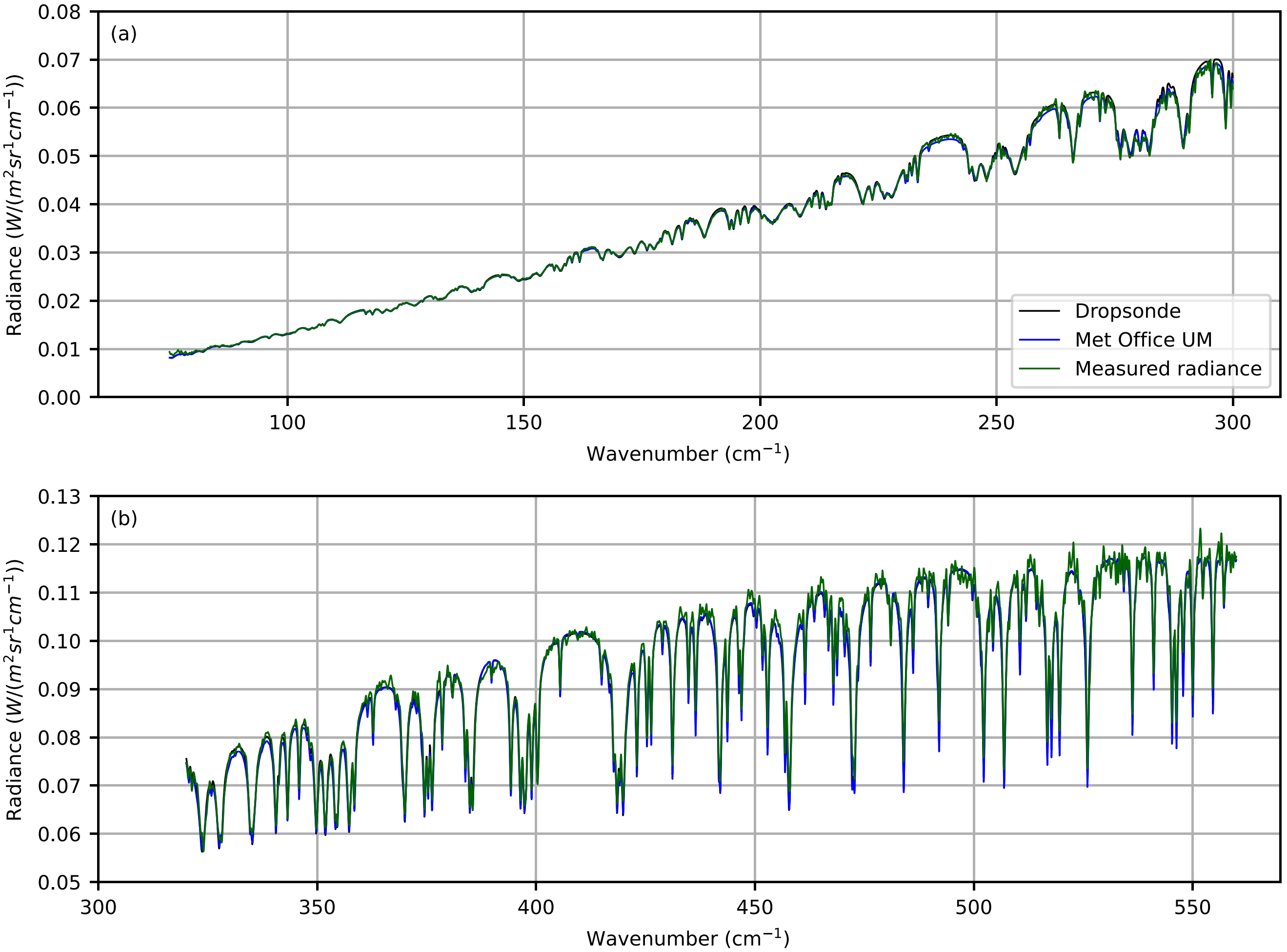

Figure 4. Simulated and observed radiance measurements taken at around 12:51 UTC, the time of dropsonde 8 release. Observations from the Tropospheric Airborne Fourier Transform Spectrometer longwave and shortwave channels are shown in panels (a) and (b) respectively.

to reconcile the simulations and observations. Detailed analysis of the TAFTS observations has not identified issues with either the instrument noise or calibration uncertainty estimates so further analysis here is restricted to TAFTS measurements at wavenumbers less than 440 cm^{-1}.

4.3. Revised Retrievals

Figure 6 shows equivalent retrievals to those performed in Section 4.1 but with the TAFTS wavenumber range reduced to 80–440 cm^{-1}. The removal of higher TAFTS wavenumbers markedly reduces the temperature bias in the bottom 2 km of the atmosphere while also improving the agreement with the dropsonde 8 between 3 and 6 km. The water vapor retrieval still follows the drier dropsonde profile between 4 and 6 km and shows improved agreement with the dropsonde between 1 and 3 km.

Table 3 shows equivalent information to Table 2 for the TAFTS retrievals illustrated in Figure 6. Compared to using the full spectral range, limiting the TAFTS range to less than 440 cm^{-1} reduces the RMSE for the temperature throughout the atmosphere, most notably between 0 and 2 km, as anticipated from Figure 6. The RMSE is also reduced for the water vapor profile at all heights below 6 km, with this reduction also manifested when considering the profile as a whole. As might be anticipated, the reduction in spectral range does result in a reduction in DFS for the reduced spectral range retrievals relative to the full range retrievals, but the difference is less than 0.2 for both temperature and water vapor (Table 4). The DFS for skin temperature are dramatically reduced, indicating that only the largest TAFTS wavenumbers are sensitive to the surface. The averaging kernels

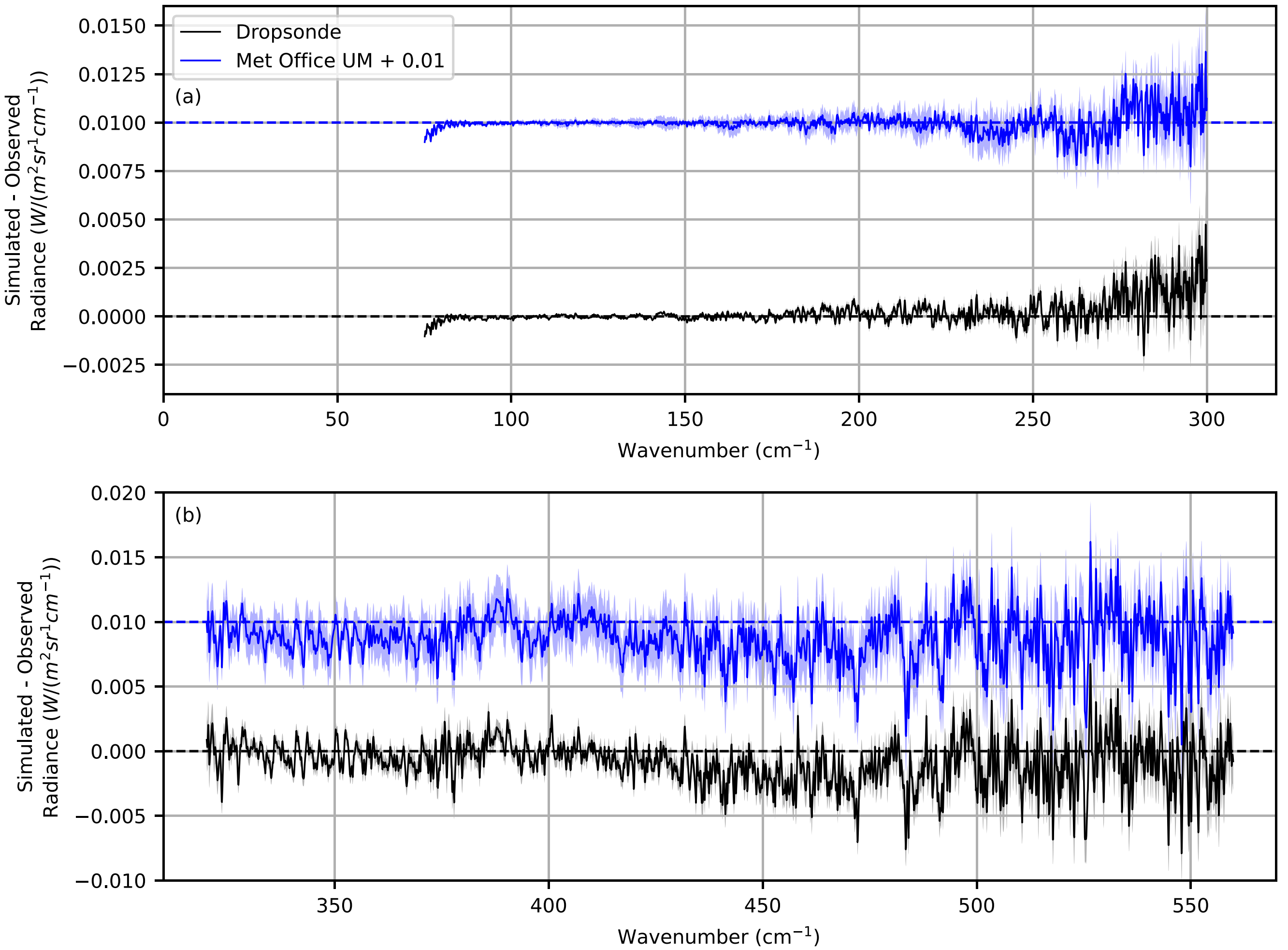

Figure 5. Radiance differences between dropsonde (black)/Met Office UM (blue) and Tropospheric Airborne Fourier Transform Spectrometer (TAFTS) observations for (a) TAFTS longwave and (b) TAFTS shortwave measurements. The shading around the lines represents propagated radiance uncertainty from the forward modeling added in quadrature with the TAFTS total measurement uncertainty.

for temperature and water vapor and plots of the a-posteriori error standard deviation are shown in Supporting Information Figures S2 and S3.

Assuming the dropsonde profile represents the truth, the retrievals from TAFTS demonstrably contain significant information about the water vapor profile and improve the Met Office forecast. Conversely the TAFTS retrieval cannot improve the original temperature forecast, likely due to the lack of coverage of the 15 μm CO_2 band.

5. Water Vapor and Temperature Retrievals From ARIES

Although Section 4 shows promising results using the far-ir we also consider whether the far-ir retrievals constitute an improvement over what could be gained using mid-ir observations of the same atmospheric state. In this section we address this question so far as is possible, using observations from ARIES.

5.1. Initial Retrieval

Retrievals of temperature and water vapor were obtained using the approach described in Section 3 but utilizing the average of 10 ARIES spectra as the measurement vector as explained in Section 2.1.2.

Figure 7 shows the retrieved temperature and water vapor profiles. The restricted wavenumber TAFTS retrievals of Section 4.3 are shown for comparison. The most notable difference between the two sets of retrievals occurs

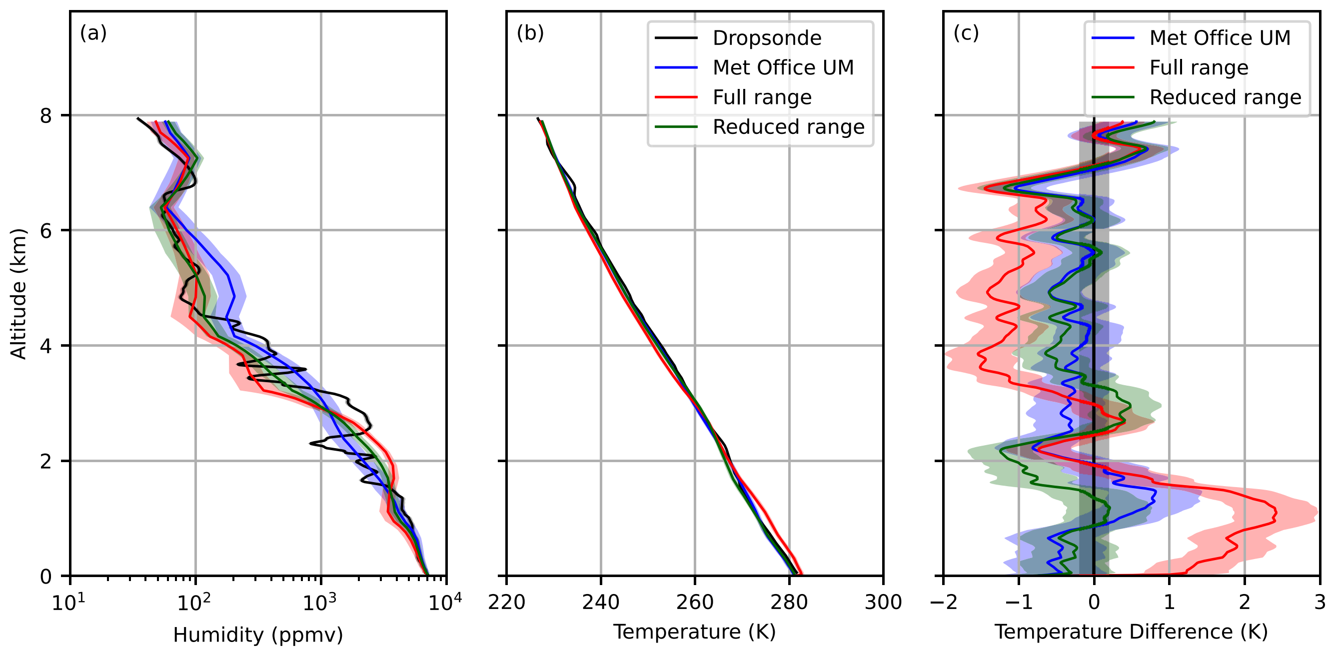

Figure 6. (a) Water vapor and (b) temperature retrievals performed using the full Tropospheric Airborne Fourier Transform Spectrometer (TAFTS) wavenumber range and using only TAFTS wavenumbers below 440 cm^{-1} (reduced range). The a-priori and dropsonde profiles are also shown. The shading around each line has the same meaning as in Figure 3. Panel (c) shows the differences of the a-priori and retrieved temperature profiles from dropsonde 8.

in the water vapor profile between 4 and 6 km, where the ARIES retrieval is much closer to the a-priori UM forecast. A second obvious difference is seen in the temperature profiles above 7 km, where the ARIES retrieval is significantly warmer than the dropsonde, the UM forecast and the TAFTS retrieval. Table 5 provides RMSE values for the ARIES retrievals. Comparison with Table 3 shows that the TAFTS retrievals are closer overall to the dropsonde measurements for both water vapor and temperature. This advantage is retained for the majority of the vertical layers considered and is also reflected in the DFS values with the ARIES values being lower than the equivalent TAFTS numbers (Table 4) at 3.03 (water vapor) and 2.41 (temperature). At first look the result for temperature is perhaps surprising given that the ARIES wavenumber range covers both the center and one wing of the CO_2 15 μm band, such that the instrument can, in theory, sound the atmospheric temperature from close to the aircraft to the surface. The averaging kernels for temperature and water vapor and plots of the a-posteriori error standard deviation for this retrieval are also shown in Supporting Information Figures S2 and S3. The water vapor averaging kernels for ARIES are generally less sharp than those for TAFTS further suggesting that the TAFTS water vapor retrieval is more sensitive to changes in the atmospheric profile.

5.2. Additional Retrievals and Forward Modeling

Given the relative performance of the ARIES and TAFTS temperature retrievals, additional investigations were undertaken to establish the cause of this behavior.

Table 3
Root Mean Squared Error Values for the Tropospheric Airborne Fourier Transform Spectrometer Reduced Wavenumber Range Retrieval

RMSE	Water vapor (log (kg/kg))	Temperature (K)
Overall	0.34	0.51
0–2 km	0.19	0.49
2–4 km	0.49	0.60
4–6 km	0.29	0.38
6–8 km	0.34	0.52

We first reduced the spectral resolution of the TAFTS spectrum from 0.24 to 1 cm^{-1} to match that of ARIES. The instrument noise from TAFTS was reduced to account for the lower resolution, and the resulting total measurement uncertainty was interpolated onto the new wavenumber grid. A retrieval of temperature and water vapor was then performed with all other parameters unchanged. The shapes of the ensuing retrievals (not shown) are very similar to those shown for the equivalent full spectral resolution TAFTS retrieval in Figures 6 and 7, indicating that the retrieval performance is not overly impacted by the reduced resolution. The DFS values are, as expected, reduced to values of 4.52 and 2.14 for water vapor and temperature, respectively. This brings the DFS for temperature lower than that for ARIES. However, the

10.1029/2020JD034229

Table 4
Degrees of Freedom for Signal Values for the Tropospheric Airborne Fourier Transform Spectrometer Retrievals at Full and Reduced Wavenumber Range

DFS	H_2O	T(z)	TSKIN
TAFTS (Full range)	5.282	2.812	0.946
TAFTS (Reduced Range)	5.129	2.640	0.035
ARIES	3.034	2.411	0.999

DFS for water vapor is still markedly higher than that for ARIES, indicating that the equivalent resolution TAFTS far-infrared observations do implicitly contain more information for water vapor than the mid-infrared observations from ARIES.

Although reducing the TAFTS spectral resolution results in the DFS for temperature from ARIES being relatively higher, still the fairly low ARIES DFS values require explanation. Forward modeling using LBLRTM was thus undertaken in a similar manner to Section 4.2, using the same "UM" and "dropsonde" profiles. Figure 8a shows the ARIES measurements and simulated radiances while Figure 8b shows the difference between the forward model and the measurements (simulated—observed). For consistency with the retrievals, the averaged ARIES spectrum and associated uncertainties are shown.

A difference of approximately 1 mW m^{-2} sr^{-1} $(cm^{-1})^{-1}$ between the two simulations is seen across the atmospheric window between 800 and 1200 cm^{-1}. This difference is driven by the surface temperature predicted by the UM forecast which is 0.6 K cooler than that derived from IREMIS and used in the dropsonde simulation. There are also marked differences between both simulations and the observations across the center of the CO_2 band from 650 to 700 cm^{-1}, a region which sounds the atmosphere very close to the aircraft. The radiances simulated in both cases are lower than those observed and show the same spectral shape. Analysis of the corresponding brightness temperatures in the CO_2 band (not shown) shows that the ARIES observations are around 3 K warmer than the air temperature measured by the in situ aircraft sensors. We believe that heating of the instrument housing, as has been observed in previous measurements (Wilson et al., 1999), may be responsible for this effect. This could explain the poor temperature retrievals produced by the ARIES measurements in the 6–8 km range, as the retrieval tries to fit the anomalously warm observations (Figure 7c).

As a final test, we explored the sensitivity of the DFS values to an artificial reduction in the calibration uncertainty associated with ARIES. Assuming a reduction of 50% results in the DFS for temperature increasing to 3.41,

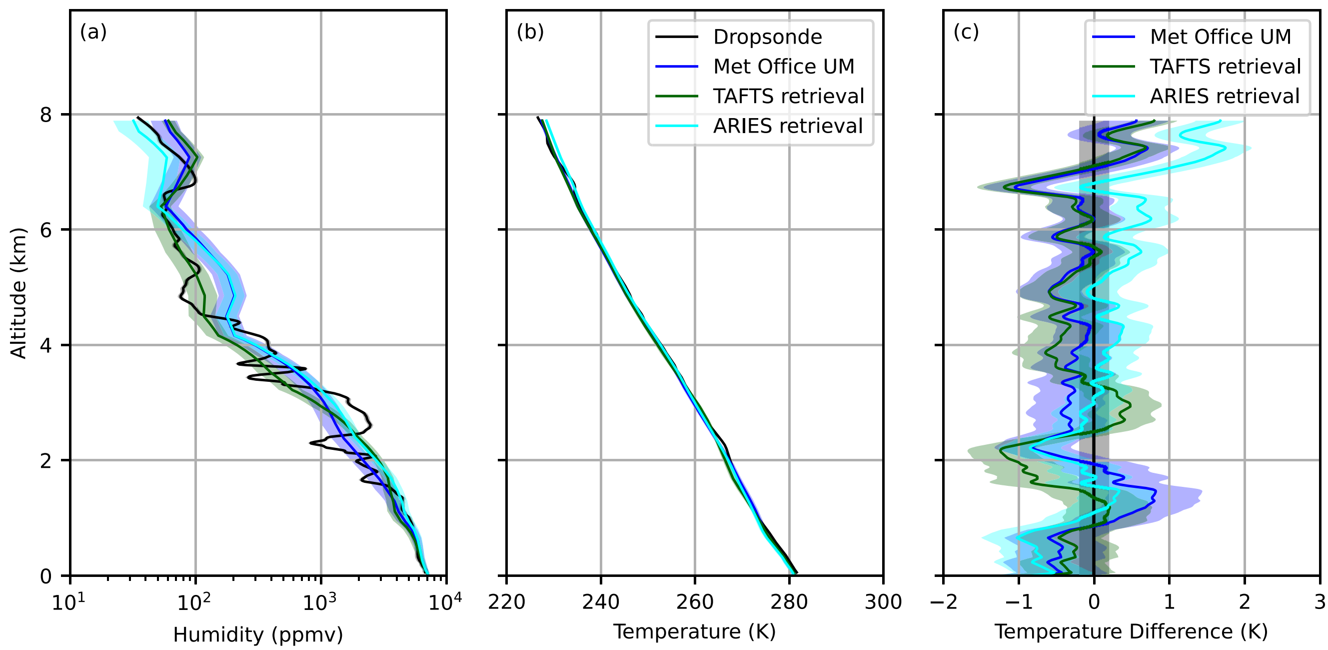

Figure 7. (a) Water vapor and (b) temperature retrievals performed using Airborne Research Interferometer Evaluation System radiances. The reduced range Tropospheric Airborne Fourier Transform Spectrometer retrievals of Section 4.3 are shown in green for comparison. The a-priori and dropsonde profiles are also shown. The shading around each line has the same meaning as in Figure 3. Panel (c) shows the differences of the a-priori and retrieved temperature profiles from dropsonde 8.

Table 5
Root Mean Squared Error Values for the Airborne Research Interferometer Evaluation System Retrievals

RMSE	Water vapor (log (kg/kg))	Temperature (K)
Overall	0.42	0.60
0–2 km	0.20	0.54
2–4 km	0.50	0.35
4–6 km	0.63	0.32
6–8 km	0.25	1.04

higher than the equivalent TAFTS value (Table 4). However, the associated RMSE of the ensuing retrievals also increases, with the retrieved temperature profile shifting further away from the dropsonde measurements. This implies that the original calibration errors associated with the measurements are realistic but high, limiting the temperature information the measurements can provide.

6. Fixed Temperature Retrievals

As our studies from Section 5.2 indicate that the ARIES spectra may be at worst unreliable and at best poorly constrained in regions of the spectrum sensitive to atmospheric temperature, we carried out further retrievals of water vapor and skin temperature only, with the atmospheric temperature profile fixed at the dropsonde measurements. Retrievals were carried out using the reduced range TAFTS spectrum, ARIES spectrum and a joint spectrum consisting of both the reduced range TAFTS spectrum and the ARIES spectrum. Figure 9 shows these retrievals.

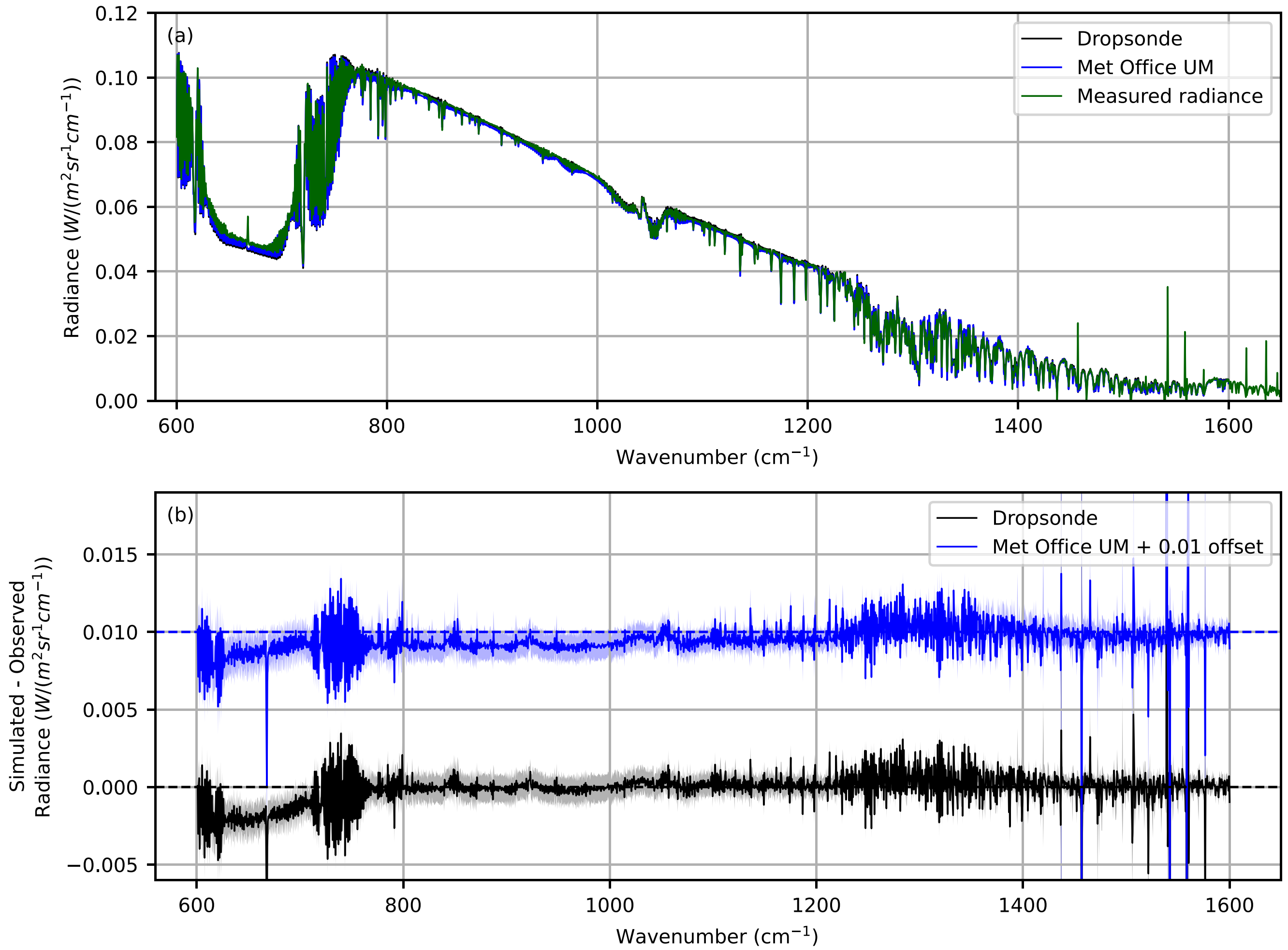

Figure 8. (a) Simulated and observed Airborne Research Interferometer Evaluation System (ARIES) radiance measurements taken at around 12:51 UTC, the time of dropsonde 8 release. (b) Radiance differences between dropsonde 8 (black)/Met Office UM (blue) simulations and ARIES observations. The shading around the lines represents propagated radiance uncertainty from the forward modeling added in quadrature with the ARIES measurement uncertainty. Both the ARIES radiances and the measurement uncertainty are representative of 10 averaged spectra.

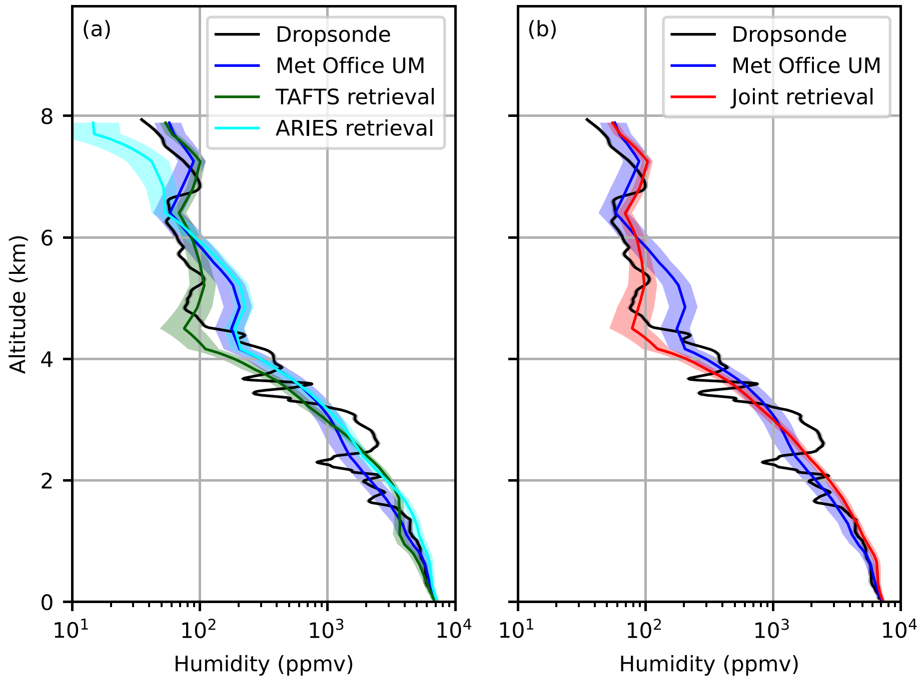

Figure 9. Water vapor only retrievals for (a) reduced range Tropospheric Airborne Fourier Transform Spectrometer and Airborne Research Interferometer Evaluation System and (b) a joint retrieval. The a-priori and dropsonde 8 profiles are also shown. The shading around each line has the same meaning as in Figure 3.

The ARIES fixed temperature retrieval does not show much improvement over the a-priori UM profile and is significantly drier than the dropsonde above 6.5 km. The TAFTS fixed temperature retrieval shows markedly lower RMSE values compared to ARIES but appears drier than the equivalent TAFTS retrieval (Figure 6a) in the 4–5 km region and this is reflected in the slightly higher RMSE value here (Table 6). Slight increases in the RMSE values are seen throughout the profile, indicating that in this case the retrieved water vapor profile has to move slightly further away from the dropsonde values to compensate for the effects of using the dropsonde temperature profile.

Combining TAFTS and ARIES in the joint retrieval significantly reduces RMSE values relative to the ARIES only case across the majority of the profile. The corollary of this is that the performance of the joint retrieval is only slightly improved relative to the TAFTS only case, with the marginal improvement also reflected in the slight increase in the number of DFS (Table 7). Overall, these results reinforce the beneficial impact that the measurement of the far-infrared radiances has for the retrieval of water vapor for this case study, particularly in the mid-upper troposphere.

Table 6
Root Mean Squared Error Values for the Water Vapor Only Retrievals

	Water vapor (log (kg/kg))			
RMSE	Met office UM	TAFTS	ARIES	Joint
Overall	0.42	0.39	0.51	0.37
0–2 km	0.11	0.23	0.26	0.21
2–4 km	0.50	0.51	0.50	0.49
4–6 km	0.63	0.42	0.72	0.36
6–8 km	0.31	0.35	0.55	0.38

7. Conclusions

In this study we have made use of measurements of clear-sky radiance from an aircraft flying in the upper troposphere to show, observationally for the first time, how far-ir radiances (in this case covering wavenumbers from 80 to 550 cm^{-1}) can be of benefit for the retrieval of mid-upper tropospheric humidity. Our work builds on previous theoretical studies which have used idealized simulations to explore the expected relative performance of instruments operating in the mid and far-ir for humidity retrieval (Merrelli & Turner, 2012; Mertens, 2002.; Ridolfi et al., 2020; Rizzi et al., 2002).

We use the retrieval framework developed specifically for the FORUM End-to-End Simulator (Sgheri et al., 2021), which has, at its heart, an optimal

10.1029/2020JD034229

Table 7
Degrees of Freedom for Signal Values for the Water Vapor Only Retrievals

DFS	H_2O	Tskin
TAFTS (Reduced range)	6.460	0.049
ARIES	3.551	1,000
Joint (TAFTS Reduced range)	6.654	1,000

estimation approach. The a-priori information for the retrievals are the closest temperature and humidity profiles in space and time taken from the UM global forecast model. Far-ir observations are from the TAFTS instrument. For the purposes of evaluation, we consider the dropsonde released from the aircraft at the time of the radiance observations to be representative of the true atmospheric state as captured by the aircraft spectrometers. Analysis of the variability in water vapor across dropsonde releases suggests that this assumption is justified for altitudes above around 4 km, although localized variability in the profile between approximately 2–3 km may compromise evaluation statistics in this region.

Initial joint retrievals of temperature and humidity using the full TAFTS spectral range showed a shift of the a-priori toward the generally drier dropsonde profile at altitudes above 4 km. However, below approximately 2 km the retrieved temperatures showed a strong bias (of up to 2 K) relative to the dropsonde profile. Forward modeling of the TAFTS radiance spectra indicated that the observed radiances in the range 440–520 cm^{-1} could not be simulated to within instrumental uncertainty, even when accounting for measurement uncertainty in the dropsonde observations. Further analysis also confirmed that realistic perturbations to surface temperature, emissivity and water vapor spectroscopy could not fully reconcile the differences. Given these findings we repeated the TAFTS retrievals restricting the wavenumber range to 80–440 cm^{-1}. The improved agreement between the retrieved and measured water vapor profile in the mid-upper troposphere was retained, with, in addition the removal of the lower-level temperature bias seen in the full range retrieval. We note that this analysis suggests that further measurements of the 440–520 cm^{-1} region are imperative in order to assess whether the radiance differences seen persist under different conditions and for alternative instrumentation.

A relevant question to pose is whether the performance of the far-ir retrieval is superior to that which could be obtained using mid-ir observations. We attempted to answer this by repeating the retrieval using the ARIES mid-ir observations from 600 to 1600 cm^{-1} as our measurement vector. Evaluation of the results showed a marked reduction in water vapor retrieval performance relative to TAFTS in terms of both root-mean-square differences with the dropsonde profiles and DFS, with the latter reducing from 5.1 to 3.0. Importantly, this advantage was not significantly affected when the TAFTS spectral resolution was degraded to match that of ARIES. A surprising result here was the relatively small DFS for temperature seen in the ARIES retrievals coupled with a strong positive temperature bias relative to the dropsonde at altitudes above 7 km. Forward modeling suggests that the bias is likely due to anomalous warming within the ARIES instrument housing, which is manifested most obviously across the center of the 15 micron CO_2 band. This further analysis also implies that the high calibration uncertainty associated with the ARIES radiances is primarily responsible for the low DFS for temperature seen in the retrievals.

Given these issues, we performed one set of final "water vapor only" retrievals, fixing the temperature profile to that observed by the dropsonde. Here again, the far-ir TAFTS retrievals substantially out-performed those from ARIES, both in terms of RMSE and DFS. This was also demonstrated by a combined retrieval, which used both the far and mid-ir observations simultaneously. The improvement in water vapor retrieval performance for this combined approach was marginal when compared to the TAFTS far-ir only case, coupled with a small increase in DFS from 6.5 to 6.7.

As discussed by Merrelli and Turner (2012) the relative measurement uncertainty in the far and mid-ir is critical in determining whether humidity retrievals inferred from far–ir observations can outperform those inferred from the mid-ir. While assuming equivalent measurement noise in both the far-ir and mid-ir results in improved information content for far-ir humidity retrievals, they argue that current technical capability is most compatible with a "high-noise" far-ir and a "low-noise" mid-ir design. In their study this implies a far-ir instrument noise that is of the order at least twice that in the mid-ir, and in this case they show that the mid-ir information content for humidity retrievals is higher. In our study, measurement uncertainties on a single spectrum in the far-ir are comparable to those of the averaged spectra used in the mid-ir, excluding wavenumbers below ~250 cm^{-1} where the far-ir uncertainty is smaller. Exploiting this real instrument configuration, our results show much improved humidity retrievals utilizing the far-ir as compared to considering the mid-ir in isolation. Given its expected noise performance (Figure 1) we expect this advantage to be retained for water vapor retrievals using far and mid-ir measurements solely from the FORUM Sounding Instrument.

Acknowledgments
L. Warwick was funded by a CASE partnership between EPSRC and the National Physical Laboratory (Grant No. EP/R513052/1). H. Brindley was funded as part of NERC's support of the National Centre for Earth Observation under Grant No. NE/R016518/1. The PIKNMIX-F flight campaign was jointly funded by the Met Office and the ESA. Airborne data was obtained using the BAe-146-301 Atmospheric Research Aircraft flown by Airtask Ltd and managed by FAAM Airborne Laboratory, now jointly operated by UKRI and the University of Leeds. The authors would like to thank the instrument operators, aircrew, operations staff, and engineers for their support during the campaign.

Data Availability Statement

Airborne data including radiance measurements are available from: Facility for Airborne Atmospheric Measurements; Natural Environment Research Council; Met Office (2019): FAAM C153 PIKNMIX-F flight: Airborne atmospheric measurements from core and non-core instrument suites on board the BAE-146 aircraft. Centre for Environmental Data Analysis, https://catalogue.ceda.ac.uk/uuid/6a2bc7a1edc34650bd41e0f958cbd50a.

References

Allan, R. P., Ramaswamy, V., & Slingo, A. (2002). Diagnostic analysis of atmospheric moisture and clear-sky radiative feedback in the Hadley Centre and Geophysical Fluid Dynamics Laboratory (GFDL) climate models. *Journal of Geophysical Research*, *107*(D17), ACL 4. https://doi.org/10.1029/2001jd001131

Anderson, G. P., Clough, S. A., Kneizys, F. X., Chetwynd, J. H., & Shettle, E. P. (1986). *AFGL (Air Force Geophysical Laboratory) atmospheric constituent profiles 0. 120km*. Air Force Geophysics Lab. (Technical Report AFGL-TR-86-0110). Hanscom AFB.

BAE Systems. (2000). *Certificate of airworthiness report no. 210: Reduced vertical separation minimum (RVSM)*. (Technical Report MFT-E-R-460-3696.).

Brindley, H. E., & Harries, J. E. (1998). The impact of far IR absorption on clear sky greenhouse forcing: Sensitivity studies at high spectral resolution. *Journal of Quantitative Spectroscopy and Radiative Transfer*, *60*(2), 151–180. https://doi.org/10.1016/s0022-4073(97)00152-0

Canas, T. A., Murray, J. E., Harries, J. E., & Haigh, J. D. (1997). Tropospheric airborne Fourier Transform spectrometer (TAFTS). *Satellite Remote Sensing of Clouds and the Atmosphere II*, *3220*, 91–102. https://doi.org/10.1117/12.301139

Chou, M. D., Weng, C. H., & Lin, P. H. (2009). Analyses of FORMOSAT-3/COSMIC humidity retrievals and comparisons with AIRS retrievals and NCEP/NCAR reanalyses. *Journal of Geophysical Research: Atmospheres*, *114*, D00G03. https://doi.org/10.1029/2008jd010227

Chung, E.-S., Soden, B. J., Sohn, B.-J., & Schmetz, J. (2014). Upper-tropospheric moistening in response to anthropogenic warming. In *Proceedings of the National Academy of Sciences of the United States of America*, *111*(32), 11636–11641. https://doi.org/10.1073/pnas.1409659111

Clough, S. A., Iacono, M. J., & Moncet, J.-L. (1992). Line-by-line calculations of atmospheric fluxes and cooling rates: Application to water vapor. *Journal of Geophysical Research*, *97*(D14), 15761–15785. https://doi.org/10.1029/92jd01419

Clough, S. A., Shephard, M. W., Mlawer, E. J., Delamere, J. S., Iacono, M. J., Cady-Pereira, K., et al. (2005). Atmospheric radiative transfer modelling: A summary of the AER codes. *Journal of Quantitative Spectroscopy and Radiative Transfer*, *91*(2), 233–244. https://doi.org/10.1016/j.jqsrt.2004.05.058

Dessler, A. E., Zhang, Z., & Yang, P. (2008). Water-vapor climate feedback inferred from climate fluctuations, 2003–2008. *Geophysical Research Letters*, *35*(20), L20704. https://doi.org/10.1029/2008gl035333

Dirksen, R. J., Sommer, M., Immler, F. J., Hurst, D. F., Kivi, R., & Vömel, H. (2014). Reference quality upper-air measurements: GRUAN data processing for the Vaisala RS92 radiosonde. *Atmospheric Measurement Techniques*, *7*(12), 4463–4490. https://doi.org/10.5194/amt-7-4463-2014

Dlugokencky, E. J., Mund, J. W., Crotwell, A. M., Crotwell, M. J., & Thoning, K. W. (2019). *Atmospheric carbon dioxide dry air mole fractions from the NOAA ESRL carbon cycle cooperative global air sampling Network 1968-2018*. Version: 2019-07. https://doi.org/10.15138/wkgj-f215

ESA. (2019) *Report for Mission Selection*: FORUM, European Space Agency, ESA-EOPSM-FORM-RP-3549, 263

FAAM Instrument Team. (2019). *FAAM instrument reference guide. (Document number FAAM000005)*. Retrieved from https://www.faam.ac.uk/wp-content/uploads/2019/11/FAAM_instrument_reference.pdf

Facility for Airborne Atmospheric Measurements, Natural Environment Research Council; Met Office. (2019). FAAM C153 PIKNMIX-F flight: Airborne atmospheric measurements from core and non-core instrument suites on board the BAE-146 aircraft [Dataset]. Centre for Environmental Data Analysis. Retrieved from https://catalogue.ceda.ac.uk/uuid/6a2bc7a1edc34650bd41e0f958cbd50a

Fetzer, E. J., Read, W. G., Waliser, D., Kahn, B. H., Tian, B., Vömel, H., et al. (2008). Comparison of upper tropospheric water vapor observations from the Microwave Limb Sounder and Atmospheric Infrared Sounder. *Journal of Geophysical Research*, *113*(22), 1–17. https://doi.org/10.1029/2008jd010000

Harries, J., Carli, B., Rizzi, R., Serio, C., Mlynczak, M., Palchetti, L., et al. (2008). The far-infrared Earth. *Reviews of Geophysics*, *46*(4), 1–34. https://doi.org/10.1029/2007rg000233

Havemann, S., Thelen, J.-C., Taylor, J. P., & Harlow, R. C. (2018). The Havemann-Taylor Fast radiative transfer code (HT-FRTC): A multipurpose code based on principal components. *Journal of Quantitative Spectroscopy and Radiative Transfer*, *220*, 180–192. https://doi.org/10.1016/j.jqsrt.2018.09.008

John, V. O., Holl, G., Allan, R. P., Buehler, S. A., Parker, D. E., & Soden, B. J. (2011). Clear-sky biases in satellite infrared estimates of upper tropospheric humidity and its trends. *Journal of Geophysical Research*, *116*, D14108. https://doi.org/10.1029/2010jd015355

Kursinski, E. R., & Gebhardt, T. (2014). A method to deconvolve errors in GPS RO-derived water vapor histograms. *Journal of Atmospheric and Oceanic Technology*, *31*(12), 2606–2628. https://doi.org/10.1175/jtech-d-13-00233.1

L'Ecuyer, T. S., Drouin, B. J., Anheuser, J., Grames, M., Henderson, D. S., Huang, X., et al. (2021). The polar radiant energy in the far infrared experiment: A new perspective on polar longwave energy exchanges. *Bulletin of the American Meteorological Society*, *102*(7), E1431–E1449.

McCarthy, M. P., Thorne, P. W., & Titchner, H. A. (2009). An analysis of tropospheric humidity trends from radiosondes. *Journal of Climate*, *22*(22), 5820–5838. https://doi.org/10.1175/2009jcli2879.1

McCarthy, M. P., Titchner, H. A., Thorne, P. W., Tett, S. F. B., Haimberger, L., & Parker, D. E. (2008). Assessing bias and uncertainty in the HadAT-adjusted radiosonde climate record. *Journal of Climate*, *21*(4), 817–832. https://doi.org/10.1175/2007jcli1733.1

Merrelli, A., & Turner, D. (2012). Comparing information content of upwelling far-infrared and midinfrared radiance spectra for clear atmosphere profiling. *Journal of Atmospheric and Oceanic Technology*, *29*(4), 510–526. https://doi.org/10.1175/jtech-d-11-00113.1

Mertens, C. J. (2002). Feasibility of retrieving upper tropospheric water vapor from observations of far-infrared radiation. In *Optical spectroscopic techniques, remote sensing, and instrumentation for atmospheric and space Research IV* (p. 4485). *Proc SPIE*. https://doi.org/10.1117/12.454251

Miloshevich, L. M., Paukkunen, A., Vömel, H., & Oltmans, S. J. (2004). Development and validation of a time-lag correction for Vaisala radiosonde humidity measurements. *Journal of Atmospheric and Oceanic Technology*, *21*(9), 1305–1327. https://doi.org/10.1175/1520-0426(2004)021<1305:davoat>2.0.co;2

Miloshevich, L. M., Vömel, H., Whiteman, D. N., & Leblanc, T. (2009). Accuracy assessment and correction of Vaisala RS92 radiosonde water vapor measurements. *Journal of Geophysical Research*, *114*(D11), D11305. https://doi.org/10.1029/2008jd011565

Miloshevich, L. M., Vömel, H., Whiteman, D. N., Lesht, B. M., Schmidlin, F. J., & Russo, F. (2006). Absolute accuracy of water vapor measurements from six operational radiosonde types launched during AWEX-G and implications for AIRS validation. *Journal of Geophysical Research*, *111*(D9), D09S10. https://doi.org/10.1029/2005jd006083

Mlawer, E. J., Turner, D. D., Paine, S. N., Palchetti, L., Bianchini, G., Payne, V. H., et al. (2019). Analysis of water vapor absorption in the far-infrared and submillimeter regions using surface radiometric measurements from extremely dry locations. *Journal of Geophysical Research: Atmospheres*, *124*, 8134–8160. https://doi.org/10.1029/2018jd029508

Palchetti, L., Brindley, H., Bantges, R., Buehler, S. A., Camy-Peyret, C., Carli, B., et al. (2020). Forum: Unique far-infrared satellite observations to better understand how Earth radiates energy to space. *Bulletin America Meteorology Social*. https://doi.org/10.1175/bams-d-19-0322.1

Petzold, A., Krämer, M., Neis, P., Rolf, C., Rohs, S., Berkes, F., et al. (2017). Upper tropospheric water vapour and its interaction with cirrus clouds as seen from IAGOS long-term routine: In situ observations. *Faraday Discussions*, *200*, 229–249. https://doi.org/10.1039/c7fd00006e

Petzold, A., Thouret, V., Gerbig, C., Zahn, A., Brenninkmeijer, C. A. M., Gallagher, M., et al. (2015). Global-scale atmosphere monitoring by in-service aircraft—Current achievements and future prospects of the European Research Infrastructure IAGOS. *Tellus B: Chemical and Physical Meteorology*, *67*(1), 28452. https://doi.org/10.3402/tellusb.v67.28452

Pierrehumbert, R. T., & Roca, R. (1998). Evidence for control of Atlantic subtropical humidity by large scale Advection. *Geophysical Research Letters*, *25*(24), 4537–4540. https://doi.org/10.1029/1998gl900203

Ridolfi, M., Del Bianco, S., Di Roma, A., Castelli, E., Belotti, C., Dandini, P., et al. (2020). FORUM Earth Explorer 9: Characteristics of level 2 products and synergies with IASI-NG. *Remote Sensing*, *12*, 1496. https://doi.org/10.3390/rs12091496

Ridolfi, M., & Sgheri, L. (2011). Iterative approach to self-adapting and altitude-dependent regularization for atmospheric profile retrievals. *Optics Express*, *19*, 26696–26709. https://doi.org/10.1364/oe.19.026696

Riese, M., Ploeger, F., Rap, A., Vogel, B., Konopka, P., Dameris, M., & Forster, P. (2012). Impact of uncertainties in atmospheric mixing on simulated UTLS composition and related radiative effects. *Journal of Geophysical Research*, *117*, D16305. https://doi.org/10.1029/2012jd017751

Rizzi, R., Serio, C., & Amorati, R. (2002). Sensitivity of broadband and spectral measurements of outgoing radiance to changes in water vapor content. In *Proc. SPIE 4485, optical spectroscopic techniques, remote sensing, and instrumentation for atmospheric and space Research IV*. https://doi.org/10.1117/12.454250

Rodgers, C. D. (2000). *Inverse methods for atmospheric sounding: Theory and practice*. World Scientific.

Rothman, L. S., Gordon, I. E., Babikov, Y., Barbe, A., Chris Benner, D., Bernath, P. F., et al. (2013). The HITRAN2012 molecular spectroscopic database. *Journal of Quantitative Spectroscopy and Radiative Transfer*, *130*, 4–50. https://doi.org/10.1016/j.jqsrt.2013.07.002

Saunders, R., Hocking, J., Rundle, D., Rayer, P., Havemann, S., Matricardi, M., et al. (2017). *RTTOV-12 Science and validation report (rep. NWPSAF-MO-TV-41)*. Met Office.

Sgheri, L., Belotti, C., Ben-Yami, M., Bianchini, G., Carnicero Dominguez, B., Cortesi, U., et al. (2021). The FORUM end-to-end simulator project: Architecture and results, Atmospheric Measurement Techniques Discussions [preprint], https://doi.org/10.5194/amt-2021-196

Sherwood, S. C., Roca, R., Weckwerth, T. M., & Andronova, N. G. (2010). Tropospheric water vapor, convection, and climate. *Reviews of Geophysics*, *48*(2), RG2001. https://doi.org/10.1029/2009rg000301

Shi, L., & Bates, J. J. (2011). Three decades of intersatellite-calibrated High-Resolution Infrared Radiation Sounder upper tropospheric water vapor. *Journal of Geophysical Research*, *116*, D04108. https://doi.org/10.1029/2010jd014847

Soden, B. J., & Bretherton, F. P. (1993). Upper tropospheric relative humidity from the GOES 6.7 μm channel: Method and climatology for July 1987. *Journal of Geophysical Research*, *98*(D9), 16669–16688. https://doi.org/10.1029/93jd01283

Trent, T., Schröder, M., & Remedios, J. (2019). GEWEX water vapor assessment: Validation of AIRS tropospheric humidity profiles with characterized radiosonde soundings. *Journal of Geophysical Research: Atmospheres*, *124*(2), 886–906. https://doi.org/10.1029/2018jd028930

Vaisala. (2017). *Vaisala dropsonde RD94*. Retrieved from https://www.vaisala.com/sites/default/files/documents/RD94-Datasheet-B210936EN-B.pdf

Vogel, B., Günther, G., Müller, R., Grooß, J.-U., Hoor, P., Krämer, M., et al. (2014). Fast transport from southeast Asia boundary layer sources to northern Europe: Rapid uplift in typhoons and eastward eddy shedding of the Asian monsoon anticyclone. *Atmospheric Chemistry and Physics*, *14*(23), 12745–12762. https://doi.org/10.5194/acp-14-12745-2014

Walters, D., Boutle, I., Brooks, M., Melvin, T., Stratton, R., Vosper, S., et al. (2017). The Met Office unified model global atmosphere 6.0/6.1 and JULES global land 6.0/6.1 configurations. *Geoscientific Model Development*, *10*(4), 1487–1520. https://doi.org/10.5194/gmd-10-1487-2017

Wilson, S. H. S., Atkinson, N. C., & Smith, J. A. (1999). The development of an airborne infrared interferometer for meteorological sounding studies. *Journal of Atmospheric and Oceanic Technology*, *16*(12), 1912–1927. https://doi.org/10.1175/1520-0426(1999)016<1912:TDOAAI>2.0.CO;2